Inversion of Speckle Interferometer Fringes for Hole-drilling Residual Stress Determinations

by D. R. Schmitt and R. W. Hunt

ABSTRACT—Speckle interferometric fringe patterns record stress-relief displacements induced by the drilling of blind-holes into prestressed objects. The quantitative determination of residual stress states from such stress patterns is difficult because of the ambiguity in the order of the observed fringes. The plane stress magnitudes are provided directly from selected fringe positions using a stochastic, iterative least squares minimization approach. The inversion requires prior knowledge of the experimental geometry and an appropriate uniaxial stress-relief displacement basis function derived from three-dimensional finite element calculations. Superpositioning of the rotated and scaled displacement basis functions allows the stress-relief relaxation for any biaxial state of stress to be determined. In this paper, fringe patterns were forward modeled from a large ensemble of calculated biaxial stress-relief displacement fields. Inversion of these noise-free fringe patterns reproduced the biaxial stresses with negligible error. Analysis of more realistic fringe patterns that include speckle noise gave stress magnitude errors that diminished rapidly with the number of selected points to better than 3 percent for 100 points. Sensitivity of the optical method is influenced by a number of factors, but the ensemble of model fringe patterns studied indicates that the stress magnitudes (normalized with respect to the material's Young's modulus) from 3×10^{-4} to 10^{-2} can accurately be determined with visible laser radiation. The method is amenable to automation and can easily be extended to study near surface gradients in the residual stresses or applied to other optical recording techniques such as moiré and phase-shifting interferometry.

KEY WORDS—

Introduction

The hole-drilling strain gage method[1] for determining residual stresses is well accepted.[2] In the method, stress-relief strains induced by the drilling of a small hole into the surface of a stressed object are recorded with a specially designed strain gage rosette.[3] Stress magnitudes and directions are determined from the observed strains using knowledge of the material's elastic properties and an appropriate stress-strain model. Tests of the method indicate strain coefficients derived from finite element modeling reproduce stress magnitudes to better than 5 percent.[4]

D. R. Schmitt (SEM Member) is a Professor, and R. W. Hunt is a Research Associate, Institute of Geophysical Research, Department of Physics, University of Alberta, Edmonton, Alberta, Canada T6G 2J1.

Original manuscript submitted: July 30, 1998.
Final manuscript received: November 15, 1999.

Despite this success, complementary efforts have focused on developing optical interferometry[5–7] in recording the submicron stress-relief displacements.[8–12] Optical methods are desirable because information is obtained over the entire field of view, the object need only be appropriately illuminated, and little, if any, surface preparation is required. This is advantageous in situations where strain gages cannot be attached. A fringe pattern image is the raw result of such methods (see Fig. 1). The shape and density of the fringes relate directly to the stress-relief deformations and, in principle, may be interpreted to yield stress magnitudes.

There are a number of complementary optical techniques that may be employed to record the information. Essentially, the fringe patterns are maps of the wrapped change in the phase of the monochromatic wave field of the light scattered from the deforming surface of the object under study. Some of the most popular methods of recording the wave fields include double exposure holography,[6] moiré interferometry,[7] electronic speckle interferometry[5] and phase-shifted speckle interferometry.[12–15] Each of the different, but complementary, methods has its advantages and disadvantages for different applications.

Double exposure holography (DEH) is perhaps the oldest of the techniques,[6] and continues to be used today.[16–18] In its simplest form, two holograms of an object before and after motion of its surface are recorded on the same piece of film. Reconstruction of the interference of these two wave fields produces a series of fringe patterns superimposed on the three-dimensional image of the object. Analysis of the fringe patterns can allow for determination of displacements on the order of one-quarter or better of the wavelength of the light employed. As with the example in Fig. 1, the shape and density of the fringes is directly related to the displacement field on the surface of the object; but the advantage of DEH is that fringes are often well resolved relative to the noisier pattern of Fig. 1. Some disadvantages of DEH are, however, that added steps of image digitization may be required and that constructing the necessary geometry of reference and object beams can be difficult in constrained locations. DEH has been employed by a number of groups attempting to quantitatively determine stress magnitudes using the hold-drilling method.[8,16–18]

In moiré interferometry,[7] a diffraction grating, typically 1200 lines/mm, is mounted or scribed on the surface of the object to be studied. The object is illuminated under two opposing, collimated beams both incident on the object at the same angle. Under this geometry, the angle of intersection between the two beams is zero and a uniform intensity is

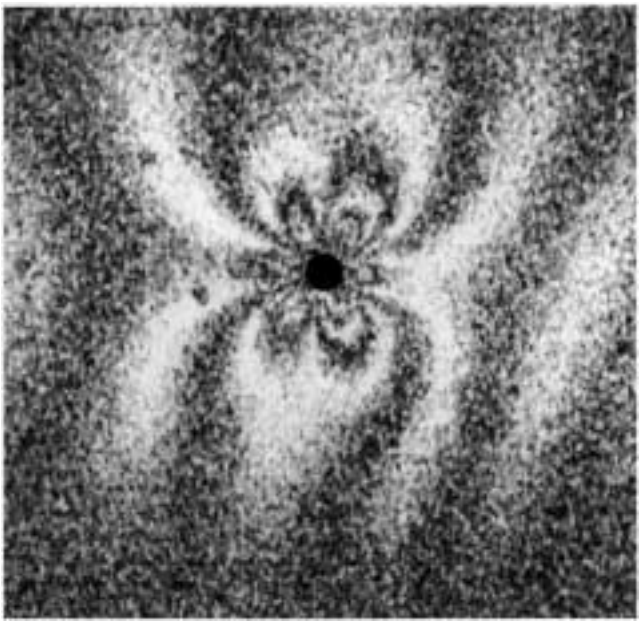

Fig. 1—Speckle interferometer fringe pattern obtained from drilling a 10 mm diameter hole into an acrylic block subject to a uniaxial vertical compression of 3.16 MPa

observed. However, once the object is deformed, the angle of intersection is no longer zero and the two diffracted wave fields interfere to form a fringe pattern. Moiré fringe patterns have good signal-to-noise ratios and are well resolved such that an accuracy of $\pm 0.02\mu$m is possible. In the hole-drilling application, this is particularly useful near the stress-relieving hole where the displacements change most rapidly and contain the most information,[10−12] making the method particularly well suited for measuring the subtle changes due to the gradient in stress from the surface of the object. One constraint on this method is that the diffraction grating must be placed on the object in the area to be studied; this may require special machining of the object or the placement of a prepared diffraction grating using epoxies that could influence the experiment.

Another method finding wide application is electronic speckle interferometry (ESPI), in which slight changes in the speckle pattern produced by motion of the object between two video frames provide the basic information. The method exploits the fact that each speckle on the surface of an object illuminated with coherent radiation is an interferometer whose intensity varies cyclically depending on the change in the phase of the light scattered from the location of the speckle. Consequently, the wrapped phase is determined by local correlations of the observed speckle pattern. The advantages of this method are as follows: there is considerable latitude for placement of source beams and the observing camera, little or no surface preparation is required and the method is inexpensive to implement.

Relative differences in the phase are easily determined from fringe patterns, but the great disadvantage of the above optical methods is that the actual value of the fringe order N cannot unambiguously be assigned without additional information. This has hindered more quantitative use of many of the optical methods, and sophisticated experimental procedures have been developed to overcome this limitation.[13−15] For example, the phase ambiguity is partially resolved in phase-shifting speckle interferometry (PSI),[13] which is a modified version of ESPI. In one early version of PSI, a spherically expanded coherent reference beam illuminates directly the surface of the CCD detector upon which the object under study is imaged. The object beam is directed to the CCD detector via a mirror mounted on a piezoelectric material whose motion can be carefully controlled; by moving the mirror, one can effect shift in the phase of the object beam. At a given deformation state, four individual speckle patterns are obtained, each acquired while the mirror is shifted through a number of predetermined motions. The wrapped phase (modulo 2π) is then given directly by a simple formula, and producing this phase is the major advantage of such a technique. Despite this advantage, the relative (unwrapped) phase must be obtained by adding or subtracting 2π from individual pixels until the phase difference between adjacent pixels in the image is less than π. Without additional information, even PSI cannot provide directly the value, in the absolute sense, of the change in the phase that is required for quantitative measurements. However, the technique described here can be applied equally as well to the relative wrapped phase maps produced by PSI.

In the context of hole-drilling stress measurements, a variety of schemes that include fringe pattern forward modeling[8,17] and fringe counting[16] have been employed to address this problem. However, there remains room for improvement on these techniques, especially given recent advances in computational power and access to powerful image-processing capabilities.

In this paper, a new method to directly invert information derived from speckle interferometer fringe patterns obtained in a hole-drilling residual stress test is developed. The method requires that an appropriate basis model of stress-relief exist. The relevant backgrounds for the displacement model and a new method of calculating speckle interferometer fringe patterns that provides information on the phase modulo 2π are reviewed and lead to a presentation of the inversion methodology in this context. The method is tested on a large ensemble of calculated fringe patterns to provide estimates of error and sensitivity. The results of this theoretical parametric study suggest that the method shows promise for the analysis of fringe patterns obtained from ESPI and moiré experiments and from the phase map resulting from PSI measurements.

Stress-relief Displacement Model

Except for special cases, the optical methods employed are all sensitive to some degree to the complete three-dimensional field of the stress-relief displacements. This complicates the analysis in that obtaining such a displacement model is problematic and usually requires that numerical methods be employed on a case-by-case basis.[17−18] For this study, a previously described[19] and experimentally tested finite element model of stress-relief displacements is used; as such, the model need only be briefly presented here. Essentially, the finite element model consisted of a block symmetric with respect to one quadrant around the stress-relief hole. The model mesh had 1782 nodes of 1352 eight-node isoparametric elements with orthotropic material properties and was calculated using ANSYS software.

For the sake of clarity, only the case in which a uniform state of biaxial plane stress parallel to the flat surface of the object will be considered. Relative to an (x, y, z)

Cartesian coordinate system (Fig. 2), this stress state is described by one shear stress τ_{xy} and two normal stresses σ_x and σ_y, with compression assumed to be positive. To aid later formulations, these three stresses will be represented as a vector $\sigma = (\tau_{xy}, \sigma_x, \sigma_y)$. At any point on the object's surface outside the hole, the complete three-dimensional biaxial stress-relief displacements are described by the vector $\mathbf{U} = (U_x, U_y, U_z)$, which depends on the point's coordinates (x, y) or equivalently (r, θ), the magnitude of the applied stresses, the elastic properties and the hole dimensions. The latter two factors are implicit in the calculation of a case-specific finite element model and subsequently can be ignored. The relationship between position from the hole and stress magnitudes becomes crucial to this analysis, that is, $\mathbf{U} = \mathbf{U}(x, y, \sigma)$.

There exist an infinite number of potential combinations in σ, so deriving each using numerical methods is obviously impossible. Fortunately, whereas the relaxed displacements remain linearly elastic, all the required displacements can be derived by the appropriate rotations and superpositions of a single basis. This basis describes the shape of the stress-relief displacement field for the uniaxial stress σ_y applied at the azimuth $\theta = \pi/2$. The three displacement components (u_x, u_y, u_z) of this basis function $\mathbf{u}(x, y, \sigma_y)$ or equivalently $\mathbf{u}(r, \theta, \sigma_y)$, show the hole to be slightly elliptical, being compressed and expanded at azimuths of $\theta = \pi/2$ and $\theta = 0$, respectively [see Figs. 3(a) and 3(b)]. The surface normal displacement field [Fig. 3(c)] is saddle shaped. The corresponding displacements produced by σ_x are simply derived by rotation of the basis $\mathbf{u}$ by $\pi/2$. Those resulting from the shear stress τ_{xy} are similarly determined[20] from one-half the difference of $\mathbf{u}$ rotated by $\pi/4$ and $-\pi/4$. Determination of the complete biaxial stress relief displacement $\mathbf{U}$ at any point can then be written in terms of the single basis $\mathbf{u}$ explicitly in simplified matrix form $\mathbf{U}(r, \theta, \sigma) = \mathbf{S}(r, \theta)\sigma$, where the shape matrix $\mathbf{S}(r, \theta)$ is given by

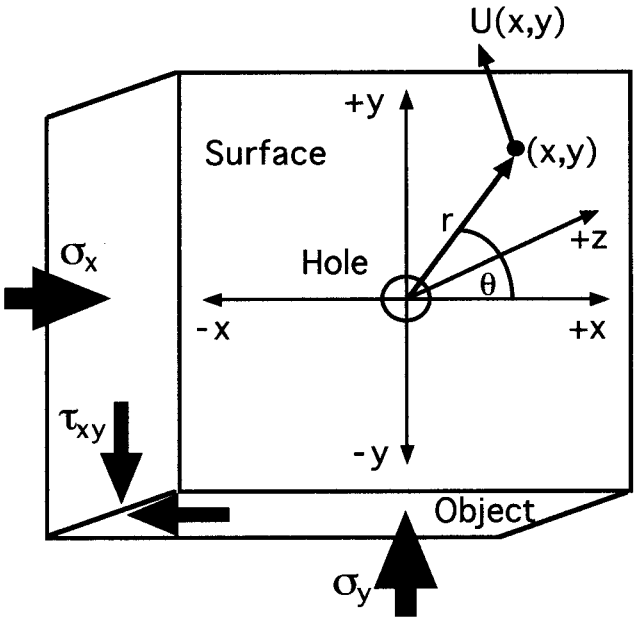

Fig. 2—Geometry of stress-relief hole in an object plate subject to a state of plane stress relative to Cartesian (x, y, z) and cylindrical (r, θ, z) coordinate systems. Hole axis coincides with the z-axis

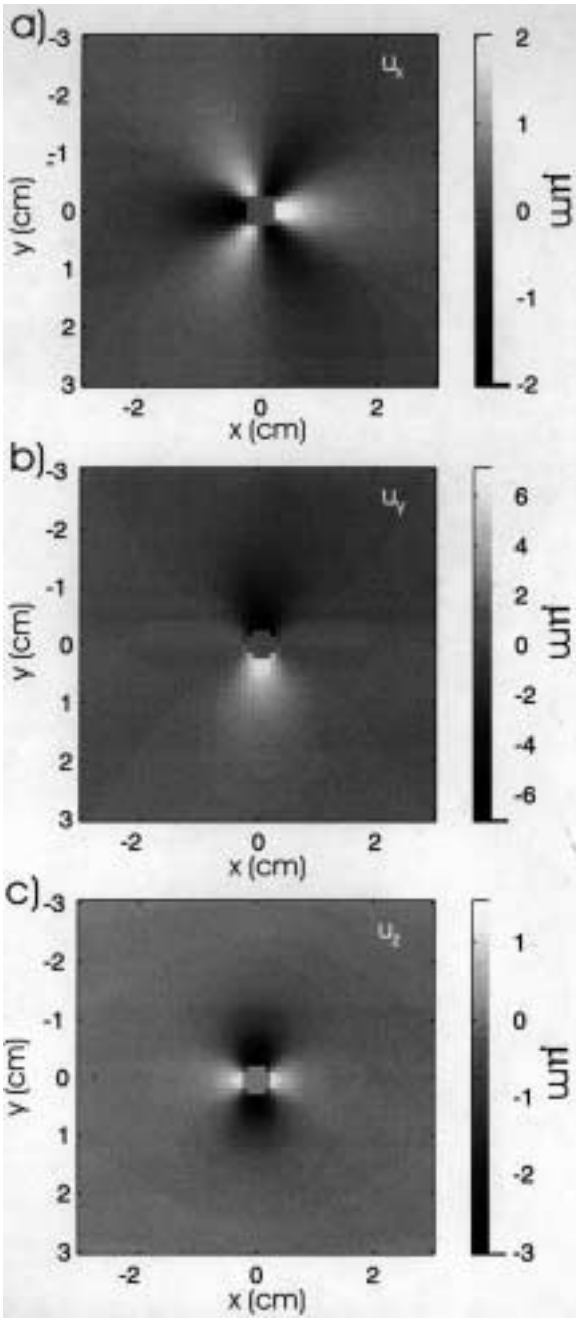

Fig. 3—Mappings of the components of the stress-relief displacement function near the drilled hole. Displacements are produced for the case of a 5 mm diameter, 10 mm deep hole drilled into a material with a Poisson's ratio of 0.4 subject to a uniaxial stress parallel to the y-axis with a magnitude of 0.002 as normalized by the material's Young's modulus

$$\mathbf{S}(r, \theta) = \begin{bmatrix} \mathbf{u}_x(r, \theta + \pi/2) & \mathbf{u}_x(r, \theta) & \frac{\mathbf{u}_x(r,\theta+\pi/4) - \mathbf{u}_x(r,\theta-\pi/4)}{2} \\ \mathbf{u}_y(r, \theta + \pi/2) & \mathbf{u}_y(r, \theta) & \frac{\mathbf{u}_y(r,\theta+\pi/4) - \mathbf{u}_y(r,\theta-\pi/4)}{2} \\ \mathbf{u}_z(r, \theta + \pi/2) & \mathbf{u}_z(r, \theta) & \frac{\mathbf{u}_z(r,\theta+\pi/4) - \mathbf{u}_z(r,\theta-\pi/4)}{2} \end{bmatrix}. \quad (1)$$

Equation (1) is useful for the inversion routine, as will be discussed.

It must be noted that the finite element method only yields directly the displacements at the nodes of the mesh used.[17] The images in Fig. 3 are interpolations (Matlab) of the irregularly spaced nodal displacements onto a rectangular grid. The interpolation procedure employed provided values only within a circular region 63.0 mm in radius centered on the stress-relieving hole's axis. In our experience, interpolation introduced negligible errors relative to those for a closed-form expression.[18] These results are based on the automatic analysis of many thousands of candidate formulas using an automated curve-fitting algorithm (TableCurve3D), with simple polynomials dependent only on r and θ.

Speckle Interferometer Fringes

We will briefly discuss the relationship between stress-relief displacements and observed fringes. More details are found in Ref. 5.

Phase and Fringe Order

In a dual-beam speckle interferometer, a coherent laser beam is split and the two arms subsequently expanded to illuminate the surface of the object (Fig. 4). The resulting speckle pattern (i.e., grainy appearance under laser light) changes cyclically with respect to the magnitude and direction of $\mathbf{U}$ and the position of the point (x, y) with respect to S_1 and S_2 as represented by unit vectors $\mathbf{n}_1$ and $\mathbf{n}_2$. This cyclical change between the speckle patterns taken immediately before and after the displacement $\mathbf{U}$ occurred is quantified as a phase angle ϕ given by

$$\phi(x, y) = \mathbf{K}(x, y) \cdot \mathbf{U}(x, y), \tag{2}$$

where $\mathbf{K}(x, y)$ is the sensitivity vector

$$\mathbf{K}(x, y) = (2\pi/\lambda)(\mathbf{n}_1(x, y) - \mathbf{n}_2(x, y)), \tag{3}$$

where λ is the wavelength of the light employed. A measure more useful to the inversion later is the fringe order N:

$$N(x, y) = \phi(x, y)/2\pi, \tag{4}$$

which at each fringe intensity peak corresponds to an integer value. At other positions, the fringe order has fractional remainders. It is worth noting that the phase in eq (2) is most sensitive to the components of $\mathbf{U}(x, y)$ parallel to $\mathbf{K}(x, y)$. This direction is nearly parallel to the surface, but because two divergent source points are employed, the direction of $\mathbf{K}(x, y)$ must vary with position. This variation is actually an advantage in the present statistical method because it aids the quality of the inversion by providing more independent measures than would be available had collimated dual beams of constant $\mathbf{n}_1$ and $\mathbf{n}_2$ been employed.

In Fig. 5, the phase for the field of displacements $\mathbf{U}$ of Fig. 3 is shown. This phase mapping determines the $\mathbf{U}(x, y)$-dependent cyclical local variations in the speckle pattern. The fringe intensity ρ in terms of ϕ is[5]

$$\rho(x, y) = (1 + \cos(\phi(x, y)))/2. \tag{5}$$

Noise-free forward-modeled fringe patterns expected for three simple different stress cases as derived from the basis displacements of Fig. 3 using eqs (2) and (5) are shown in Fig. 6.

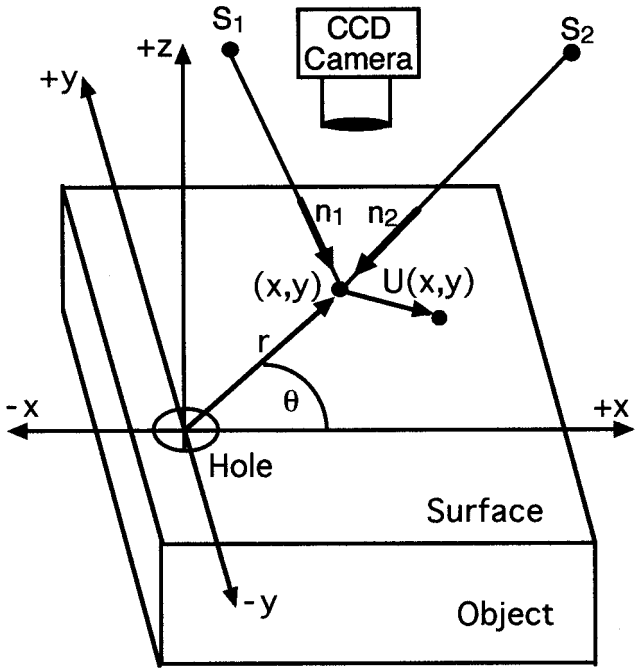

Fig. 4—Geometry of the dual-beam speckle interferometer. Arms of split coherent beam (not shown) are expanded at source points S_1 and S_2 to illuminate the surface. Unit vectors $\mathbf{n}_1$ and $\mathbf{n}_2$ indicate the directions from the source points to the surface point (x, y), which experiences total stress-relief displacement $\mathbf{U}$. Speckle patterns on the object's surface are observed using a CCD camera

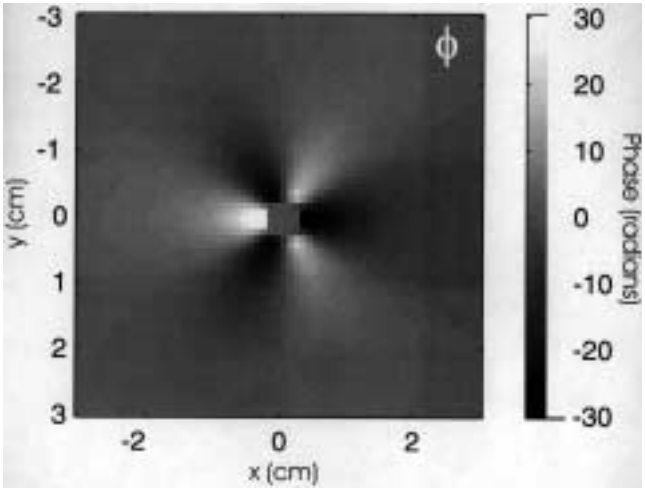

Fig. 5—Mapping of the phase ϕ of the displacement field of Fig. 3 for the red He-Ne laser 632.8 nm wavelength. Divergent (spherical) source points at (75.5 mm, 2.0 mm, 64.0 mm) and ($-$54.5 mm, 2.0 mm, and 73.0 mm)

The calculated fringe patterns in Fig. 6 and eq (5) highlight the ambiguities apparent when the fringe patterns must be interpreted. As phase increases with position [Fig. 7(a)], the corresponding fringe intensity [Fig. 7(b)] oscillates between zero and one. The absolute value and slope of the phase are lost in the fringe pattern. An observer interpreting the fringe intensities can at best determine only a relative phase to no better than an angle of π radians [Fig. 7(c)]; that is, the observer knows only that the fringe peak at $x = 0$ corresponds to a phase $\phi = 2i\pi(i = 0, \pm1, \pm2, \ldots)$ and

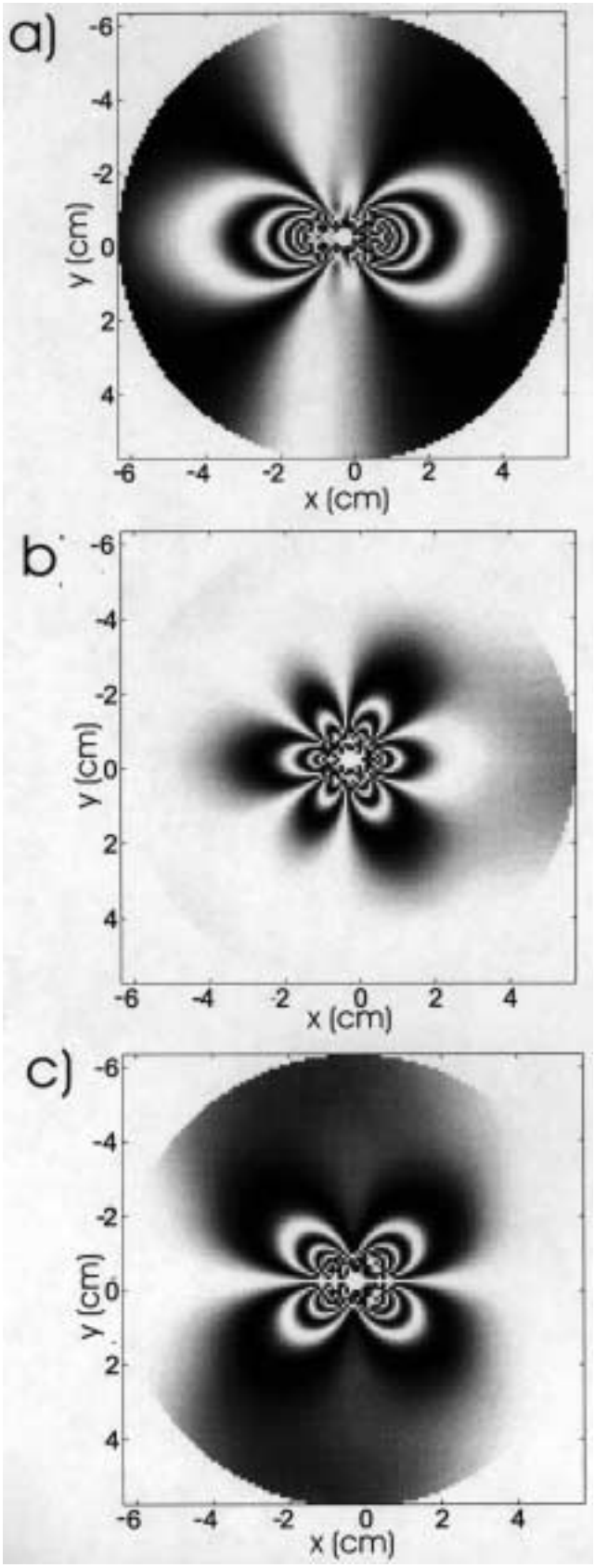

Fig. 6—Calculated noise-free fringe patterns for simple stress conditions of (a) $\sigma_x = 6$ MPa, (b) $\sigma_y = 6$ MPa and (c) $\tau_{xy} = 12$ MPa in a material with $E = 3.0$ GPa. The box containing each synthetic fringe pattern has square dimensions of 126.0 mm. The fringe pattern appears only in circular region as a result of the interpretation procedure

does not know whether the phase should be increasing or decreasing between peaks (i.e., the sign is ambiguous[6]). PSI methods provide more directly the phase ϕ but still cannot determine this phase absolutely, since only wrapped values are provided. However, if a particular displacement field is expected, the interpreter knows that variation of the phase with position and, consequently, is able to assign relative values of absolute phase to each fringe. This constraint can be used to construct a family of possible phase curves, a subset of which is illustrated by the light lines in Fig. 7(a).

In speckle interferometry, the raw data consist of two grainy speckle patterns commonly acquired before and after the deformation **U** with a digital camera (Fig. 4). The fringe pattern is calculated from these two images. Researchers[21] noted that local portions of the fringe patterns having a phase difference of $\phi = 2i\pi$ remain unchanged between the two exposures. Alternatively, if $\pi = (2i + 1)\pi$, then the local speckle pattern differs completely. Consequently, measures of the local correlation between the two images serve as proxies for the phase, and mappings of these correlations produce the fringe pattern.[5]

Traditionally, a variety of simple means to estimate this correlation between video frames were developed directly as part of a sophisticated circuit, and the technique was hence referred to as ESPI. A modified version[22] in which local values of Pearson's coefficient of correlation are mapped is used here. The advantage of this method is that the mapped correlation values are the same as those theoretically expected in eq (5) and that the method does not require ideal uniform illumination of the object. For example, the fringe pattern of Fig. 1 is the direct result of one such application and has not been digitally enhanced in any way. In the convention used, a bright fringe peak (good correlation) and a dark fringe trough (poor correlation) correspond to phases $\phi = 2i\pi$ (or a fringe order of $N = i$) and $\phi = (2i + 1)\pi$ (or a fringe order of $N = i + 1/2$), respectively.

Fringe Pattern Inversion

The plane stresses are determined directly in the inversion described here that is a specialized modification of a recently developed displacement measurement technique.[23] Briefly, the technique consists of first selecting a series of positions with the same phase (e.g., along a bright fringe peak). This set of points (manually selected in this test of the concept) is arbitrarily assigned an integer fringe order value M. Points are then selected from the peak of the next bright fringe to which a fringe order of $M + 1$ is attached. This continues with the points from the subsequent fringe, which are given a value of $M + 2$. fringes on the opposite side of the initial M-order fringe would be assigned decreasing values of $M-1$, $M - 2$, and so on. Other features of the fringe pattern such as the dark fringe troughs or the points at which the fringe change from dark to bright can also be used and correspond to fringe orders that differ from integer values by $\pm 1/2$ and $\pm 1/4$, respectively. Indeed, the more points selected, the better the statistical validity of the solution and the lower the error.

The observer must have some knowledge of the expected character of the motions so that the fringe order values may be applied in a proper systematic fashion. This is easily accomplished by studying a few forward-modeled fringe patterns

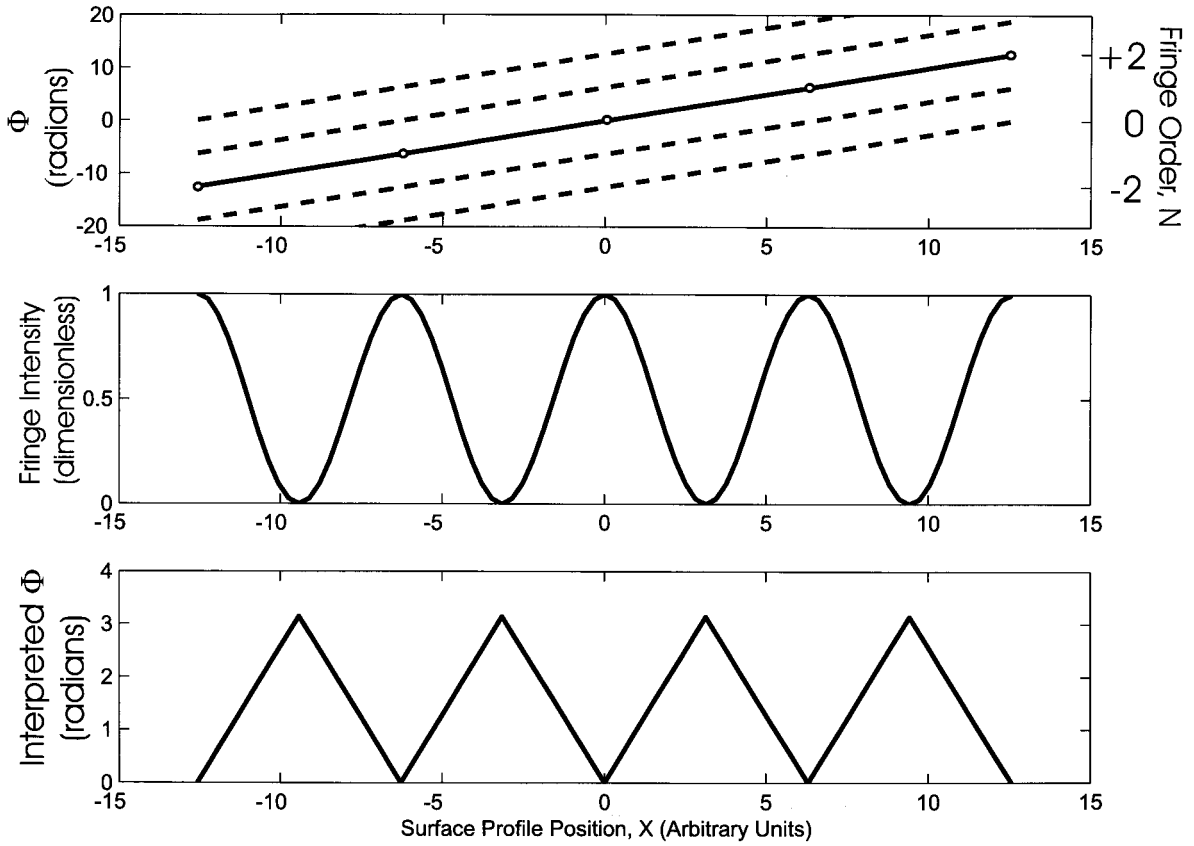

Fig. 7—Line plot through a hypothetical fringe pattern illustrating the relationship between (a) actual (heavy lines) and a subset of possible interpreted (light lines) phases (open circles represent selected bright fringe peaks), (b) observed fringe intensity and (c) ambiguity in phase in the interpretation of (b)

such those shown in Fig. 6 for which the fringe order is known a priori.

The position of the observed fringes can be determined accurately, but the initial fringe-order assignations will most likely be incorrect. These values are used, however, in a least squares calculation to determine the displacements. The error of this measurement is determined, and a second iteration of the calculation is repeated after the fringe orders have been appropriately and automatically incremented. This is equivalent to moving between the set of possible interpreted phases of Fig. 7(a). The least squares and error calculations are repeated until the minimum error is found.[17] This procedure yielded errors of better than one part in 10^4.

The method of stress determination here follows a different approach, which is developed below. Following eqs (1), (2) and (4) in the forward sense, the fringe order at any position can be written as

$$N(x, y) = [\mathbf{K}(x, y)\mathbf{S}(x, y)] \cdot \sigma/2\pi = g(x, y) \cdot \sigma. \quad (6)$$

The term $[\mathbf{K}(x, y)\mathbf{S}(x, y)]/2\pi$ reduces to a vector $\mathbf{g}(x, y)$ with components $(g_a(x, y), g_b(x, y), g_c(x, y))$, combining the known information of the experimental geometry and the shape of the basis displacements. Consequently, at each observed position, the assigned fringe order in the image is described as the vector product of a known quantity **g** and the three unknown stresses in σ to be determined.

If m points within the fringe pattern are selected, the corresponding system of equations may be written concisely in matrix form as

$$\begin{bmatrix} N(x_1, y_1) \\ N(x_2, y_2) \\ \cdot \\ \cdot \\ \cdot \\ \cdot \\ \cdot \\ N(x_m, y_m) \end{bmatrix} = \quad (7)$$

$$\begin{bmatrix} g_a(x_1, y_1) & g_b(x_1, y_1) & g_c(x_1, y_1) \\ g_a(x_2, y_2) & g_b(x_2, y_2) & g_c(x_2, y_2) \\ \cdot & \cdot & \cdot \\ \cdot & \cdot & \cdot \\ \cdot & \cdot & \cdot \\ \cdot & \cdot & \cdot \\ \cdot & \cdot & \cdot \\ \cdot & \cdot & \cdot \\ g_a(x_m, y_m) & g_b(x_m, y_m) & g_c(x_m, y_m) \end{bmatrix} \begin{bmatrix} \sigma_x \\ \sigma_y \\ \tau_{xy} \end{bmatrix},$$

or, in abbreviated form, $\mathbf{N} = \mathbf{G}\sigma$, which is readily solved with the method of least squares:[23]

$$\sigma = (\mathbf{G}^{\mathbf{T}}\mathbf{G})^{-1}\mathbf{G}^{\mathbf{T}}\mathbf{N}. \quad (8)$$

The sum of squares fringe order error, which is to be minimized in the iterative updates of **N**, is

$$E = |\mathbf{N}^2 - (\mathbf{S}\sigma)^2|. \tag{9}$$

As with the simpler translation measurements,[23] a set of rules is required to appropriately assign relative fringe order values. Briefly, the procedure relies on keying the fringe pattern according to the number of lobes (see Fig. 6), determining which is the zeroth-order bright fringe on the basis of the symmetry of the pattern and assigning within each set of fringes in a given lobe the incremental values of fringe order with approach to the stress-relieving hole boundary. This simple checklist assumes that the fringe patterns are not contained within the translational displacements and that the possibility of the existence of such motions may need to be considered. If necessary, the least squares approach is easily modified to include such movements.

Numerical Tests and Discussion

An ensemble of 32 synthetic fringe patterns randomly selected to have stresses falling within the ranges of -6 MPa $\leq \sigma_x, \sigma_y \leq 6$ MPa and -12 MPa $\leq \tau_{xy} \leq 12$ MPa were calculated using the basis displacements of Fig. 3 and eqs (1) and (5). As noted earlier, inversion of data from perfectly noise-free fringe patterns such as those of Fig. 6 yielded negligible error, indicating that numerical computation is not a significant source of uncertainty. These synthetic fringe patterns were made more realistic by simulating the random speckle noise as is seen in Fig. 1. This was accomplished by modulating the noise-free fringe patterns with a random root-mean-square value of 0.4. One such synthetic fringe pattern is shown in Fig. 8. The speckle noise results in substantial positioning errors during fringe selection as is seen by the scatter of the open circles in Fig. 8, which should follow a more continuous path. This problem is most severe far from the stress-relieving hole where the fringes are broader. In spite of this source of error, the fringe positions recreated by the inversion match the known fringe centers well.

Up to 1000 individual fringe positions were manually selected in each of the synthetic fringe patterns. This was carried out manually because we felt it prudent to test the concept prior to developing more extensive automatic fringe selection algorithms. Indeed, because of the novel correlation method used, the fringes can easily in principle be converted to phase modulo 2π via eq (5), and there is nothing to preclude the use of the entire set of pixels in the fringe pattern. In all cases, the inversion procedure yielded progressively better measures of the three applied stresses as more selected points were included. These results are summarized in Fig. 9, which shows the decay of the error between the known plane stress magnitudes and those reproduced versus number of points in each fringe pattern used in the inversion. The inversion appears quite robust, with an average stress magnitude error near 3 percent produced from the inclusion of only 100 points.

These synthetic results provide a baseline for errors that are expected to result from the inversion itself and indicate that it provides acceptable solutions. However, application of the methodology to a real hole-drilling experiment will be complicated by a number of additional factors. The most important error is use of an incorrect or insufficiently sophisticated stress-relief displacement basis model. This is a problem that afflicts all hole-drilling measurements regardless of whether optical or strain gage recording is used. Problems include transient thermal displacements from the heat of drilling,[24] time-dependent creep near the stress-relieving hole,[17,25] anisotropic or nonlinear elastic response of the material, near-surface stress gradients[26] or use of the wrong

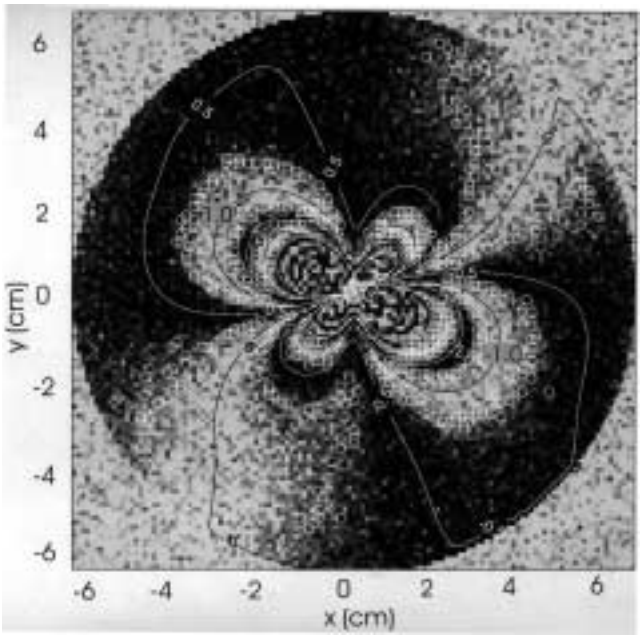

Fig. 8—One calculated fringe pattern including random speckle noise from the ensemble analyzed. Points selected for use in the inversion are shown as white open circles. White and black lines on dark and bright fringes, respectively, show the numbered fringe order contours reproduced in the inversion

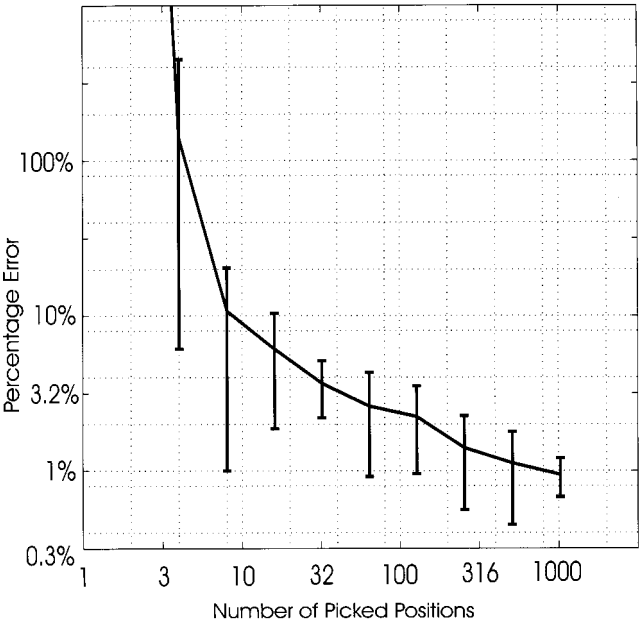

Fig. 9—Average error in stress magnitudes determined versus number of selected points used in the inversion. Error bars represent one standard deviation

elastic moduli and relative hole dimensions in the development of the basis model. Some experimental problems that can influence the quality of the inversion are errors in the determination of the relative locations of the source points, the object's surface and the hole position; and the accuracy with which the hole has been drilled. Translations and rotations of the object during drilling are another source of error, but these can be accommodated as part of the least squares solution if necessary.

Although mentioned briefly, in the context of hole-drilling, residual stress determinations and the problem of large gradients in the concentrated stresses near the surface are presently of the greatest practical importance. Incremental drilling is often used in attempts to measure shallow stress distributions.[11−12,26] The incremental drilling problem relies on the continuous monitoring of the stress-relief deformation with progressive deepening of a shallow hole; as a result, high sensitivity to small deformations near the stress relief hole is necessary. Recent developments toward this sensitivity have included both strain gage[3] and moiré interferometry.[11,12] In the latter method, a closed-form solution for the changes in the displacements with drilled hole depth was developed from finite element analysis.[11] That is, for each hole depth, a new set of calibration coefficients describing the stress-relief displacements was derived. These resulting closed-form equations are particularly well suited for application in the present least squares method. Furthermore, the time lapse capabilities[24] of the digital speckle interferometer to record nearly continuously the progressive changes in the shape of the object with hole depth could be fully exploited if an appropriate series of displacement models existed.

What range of stress magnitudes can be reasonably measured with the optical technique is an important question. Determining these bounds is not easily accomplished, since the displacements and, hence, the fringe density depend on many factors such as the elastic moduli, the hole dimensions and the wavelength of the light used. A lower bound is set by the point at which distinct fringes are no longer detectable. The upper bound is controlled by the loss of coherence and blending of fringes at high densities relative to the pixel spacing of the imaging system.[22] The result of the study of this ensemble of fringe patterns suggests, however, that stresses (as normalized by the material's Young's modulus) falling within the range of 3×10^{-4} to 10^{-2} are accurately detectable with the red He-Ne laser light.

Conclusions

The fringe inversion method developed here provides satisfactory and robust quantitative determinations of stress magnitudes in a hole-drilling residual stress measurement. One novel aspect is that ambiguities in determining the order of the fringes are overcome by an iterative recalculation that seeks the lowest error solution by progressively updating the input fringe orders. Assuming the stress-relief displacement model employed in this paper is correct, even speckle patterns contaminated with speckle noise will provide small errors of less than 3 percent for a modest number of selected points within a fringe image.

The results are encouraging, but the present method that includes manual selection of fringe positions and the assignment of fringe orders is laborious. Many of these aspects could be automated, however. For example, observed fringe pattern images are easily filtered such that the final pixel value is the theoretical value of the phase modulo 2π, providing the same initial results as produced by the phase-shifting methods[13] but without the added instrumental difficulties. At this point, the relative phase determination methods described earlier for PSI could be employed; alternatively, the initial modulo 2π phase maps produced in a PSI test could employ the iterative absolute phase assignation method described in this paper. Furthermore, the final absolute phase maps produced by the PSI method could easily be incorporated into the least squares inversion method to provide more reliable measurement of displacement if the form that the displacement field must take is already known. One possible way to further automate the determination of the absolute fringe or phase order is to use modern advanced inversion procedures such as simulated annealing, random walk processes and genetic algorithms.

The results of application of this inversion routine to the analysis of real hole-drilling fringe patterns acquired in laboratory calibrations is forthcoming.[27]

Acknowledgments

This work was supported by NSERC research and equipment grants. Dr. Y. Li provided his stress-relief displacement models for this study. L. Tober, J. Haverstock, J. MacKinnon and G. Reese were instrumental in the production of this paper. Two anonymous reviewers are thanked for pointing out some related contributions in the recent literature.

References

1. Rendler, N.J. and Vigness, I., "Hole-drilling Strain-gage Method of Measuring Residual Stresses, EXPERIMENTAL MECHANICS, **21**, *577–586 (1966).*

2. ASTM, "Standard Test Method for Determining Residual Stresses by the Hole-drilling Strain-gage Method, 1993 Annual Book of ASTM Standards, American Society of Testing and Materials (1993).

3. Schajer, G.S. and Tootoonian, M., "A New Rosette Design for More Reliable Hole Drilling Residual Stress Measurements, EXPERIMENTAL MECHANICS, **37**, *299–306 (1997).*

4. Schajer, G.S., "Application of Finite Element Calculations to Residual Stress Measurements, J. Eng. Mat. Tech., **103**, *157–163 (1981).*

5. Jones, R. and Wykes, C., Holographic and Speckle Interferometry, Cambridge University Press, Cambridge (1983).

6. Kreis, T., Holographic Interferometry—Principles and Methods, Akademie Verlag, Berlin (1996).

7. Post, D., Han, B., and Ifju, P., High Sensitivity Moiré (Experimental Analysis for Mechanics and Materials), Springer-Verlag, New York (1994).

8. Bass, J.D., Schmitt, D.R., and Ahrens, T.J., "Holographic In Situ Stress Measurements, Geophys. J. Roy. Astr. Soc., **85**, *13–41 (1986).*

9. Nelson, D.V. and McCrickerd, J.T., "Residual Stress Measurement Through Combined Use of Holographic Interferometry and Blind Hole Drilling, EXPERIMENTAL MECHANICS, **26**, *371–378 (1986).*

10. Nicoletto, G., "Theoretical Fringe Analysis for a Coherent Optics Method of Residual Stress Measurement, J. Strain Anal., **23**, *169–178 (1991).*

11. Wu, Z., Lu, J., and Han, B., "Study of Residual Stress Distribution by a Combined Method of Moiré Interferometry and Incremental Hole Drilling, Part I: Theory, ASME J. Appl. Mech., **65**, *837–843 (1998).*

12. Wu, Z., Lu, J., and Han, B., "Study of Residual Stress Distribution by a Combined Method of Moiré Interferometry and Incremental Hole Drilling, Part II: Implementation, ASME J. Appl. Mech., **65**, *844–850 (1998).*

13. Creath, K., "Phase-shifting Speckle Interferometry, Appl. Opt., **24**, *3053–3058 (1985).*

14. Johansson, S. and Predko, K.G., "Performance of a Phase-shifting Speckle Interferometer for Measuring Deformation and Vibration, J. Phys. E., **22**, *289–291 (1989).*

15. Kato, J., Yamaguchi, I., and Ping, Q., "Automatic Deformation Analysis by a TV Speckle Interferometer Using a Laser Diode, Appl. Opt., **32**, *77–83 (1993).*

16. Makino, A. and Nelson, D.V., "Residual-stress Determination by Single-axis Holographic Interferometry and Hole-drilling—Part 1: Theory, EXPERIMENTAL MECHANICS, **34**, *66–78 (1994).*

17. Schmitt, D.R. and Li, Y., "Three-dimensional Stress Relief Displacement Resulting From Drilling a Blind Hole in Acrylic, EXPERIMENTAL MECHANICS, **36**, *412–420 (1996).*

18. Makino, A., Nelson, D.V., Fuchs, E.A., and Williams, D.R., "Determination of Biaxial Residual Stresses by a Holographic—Hole Drilling Technique, J. Eng. Mat. Tech., **118**, *583–588 (1996).*

19. Schmitt, D.R. and Li, Y., "Influence of a Stress Relief Hole's Depth on Induced Displacements: Application to Interferometric Stress Determinations, Int. J. Rock Mech. Min. Sci. Geomech. Abstr., **30**, *985–988 (1993).*

20. Timoshenko, S.P. and Goodier, J.N., Theory of Elasticity, McGraw-Hill, New York (1970).

21. Leendertz, J.A., "Interferometric Displacement Measurement on Scattering Surfaces Utilizing Speckle Effect, J. Phys. E. Instrum., **3**, *214–218 (1970).*

22. Schmitt, D.R. and Hunt, R.W., "Optimization of Fringe Pattern Calculation with Direct Correlations in Speckle Interferometry, Appl. Opt., **36**, *8848–8857 (1997).*

23. Schmitt, D.R. and Hunt, R.W., "Model-based Inversion of Speckle Interferometer Fringe Patterns, Appl. Opt., **37**, *2573–2578 (1998).*

24. Schmitt, D.R. and Hunt, R.W., "Time-lapse Speckle Interferometry, Geophys. Res. Lett. (1999).

25. Whitney, T.S. and Stener, G.J., "A Device for Implementing the Strain Gage-hole Drilling Method of Residual Stress Measurement on Aircraft Transparencies, Exp. Tech., 25–30 (Jul.-Aug. 1993).

26. Makino, A. and Nelson, D.V., "Determination of Subsurface Distributions of Residual Stress by a Holographic-hole Drilling Technique, J. Eng. Mat. Tech., **119**, *95–103 (1997).*

27. Schmitt, D.R. and Hunt, R.W., "Determination of Residual Stress by Inversion of Speckle Interferometer Fringe Patterns: Experimental Tests, Unpublished manuscript (1999).